In vivo anticancer activity of a rhodium metalloinsertor in the HCT116 xenograft tumor model

Stephanie D. Threatt[a], Timothy W. Synold[b], Jun Wu[c], and Jacqueline K. Barton[a,1]

[a]Department of Chemistry and Chemical Engineering, California Institute of Technology, Pasadena, CA 91125; [b]Department of Medical Oncology & Therapeutics Research, City of Hope, Duarte, CA 91010; and [c]Center for Comparative Medicine, City of Hope, Duarte, CA 91010

Contributed by Jacqueline K. Barton, May 18, 2020 (sent for review April 8, 2020; reviewed by Jonathan L. Sessler and Brian M. Zeglis)

Mismatch repair (MMR) deficiencies are a hallmark of various cancers causing accumulation of DNA mutations and mismatches, which often results in chemotherapy resistance. Metalloinsertor complexes, including [Rh(chrysi)(phen)(PPO)]Cl_2 (Rh-PPO), specifically target DNA mismatches and selectively induce cytotoxicity within MMR-deficient cells. Here, we present an in vivo analysis of Rh-PPO, our most potent metalloinsertor. Studies with HCT116 xenograft tumors revealed a 25% reduction in tumor volume and 12% increase in survival with metalloinsertor treatment (1 mg/kg; nine intraperitoneal doses over 20 d). When compared to oxaliplatin, Rh-PPO displays ninefold higher potency at tumor sites. Pharmacokinetic studies revealed rapid absorption of Rh-PPO in plasma with notable accumulation in the liver compared to tumors. Additionally, intratumoral metalloinsertor administration resulted in enhanced anticancer effects, pointing to a need for more selective delivery methods. Overall, these data show that Rh-PPO inhibits xenograft tumor growth, supporting the strategy of using Rh-PPO as a chemotherapeutic targeted to MMR-deficient cancers.

metal–DNA | DNA mismatch | cancer | metal therapeutic

Metal complexes have long been used to target DNA in order to achieve efficient cytotoxicity in cancerous cells (1–4). Several of the leading chemotherapeutic drugs, such as cisplatin and oxaliplatin, are metal complexes that irreversibly bind DNA and inhibit DNA replication. Due to the efficacy of these therapeutics, 10 to 20% of all cancer patients are prescribed platinum-based drugs (5). While these platinum complexes successfully cause cell death within cancerous tissues, they also result in toxicity toward healthy, often rapidly dividing, cells, leading to side effects that include gastrointestinal toxicity and nephrotoxicity (6, 7). Additionally, the majority of patients treated with these classic DNA-targeted chemotherapeutics develop resistance, which causes these therapies to lose effectiveness (8–10). As a result, much research has shifted focus toward developing chemotherapeutics with improved selectivity for killing tumor cells (11).

Our laboratory has designed transition metal complexes that specifically target DNA base-pair mismatches, such as those that occur with polymerase errors during DNA replication. While in healthy, normal cells these mismatches are repaired by the mismatch repair (MMR) protein machinery, certain cancerous tissues have malfunctioning MMR, which causes mismatch sites to persist, ultimately yielding increased mutations and enhanced cancerous transformations (12). MMR deficiencies are a hallmark for ∼15% of colorectal cancer cases and up to 20% of all solid tumors. Colorectal cancer patients often undergo genetic screens, including for MMR mutations and microsatellite instability, which help to guide clinical treatment decisions (13, 14). Low responsiveness is often apparent with traditional chemotherapeutics including fluoropyrimidines and platinum therapy, particularly leading to the buildup of resistance. Recently it has been found that MMR-deficient patients may be responsive to anti–PD-1/PD-L1 immunotherapies (15); while developments with immunotherapies have been promising for treating MMR-deficient cancers, there is still a strong need for additional therapeutic options.

Designing metal complexes capable of selectively targeting the DNA mismatches that are associated with MMR-deficient cancers and exploring their biological activity has been an objective of our group and others (16, 17). We have developed transition metal complexes, specifically rhodium compounds, that bind to thermodynamically destabilized DNA mismatch sites via a binding mode termed metalloinsertion. In this binding mode, the metal complex inserts at the site of the mismatched base pair via its planar and sterically expansive inserting ligand chrysi (5,6-chrysenequinone diimine), resulting in the ejection of the destabilized mismatch base pair from the DNA helix (18, 19).

Early-generation metalloinsertor complexes, such as $[Rh(bpy)_2(chrysi)]^{3+}$, were characterized by an all N^N coordination environment and initial studies with these metalloinsertors revealed highly selective binding to mismatch sites. Remarkably, the in vitro mismatch binding of metalloinsertors translated into selective cellular properties, in which preferential inhibition of cellular proliferation was observed for MMR-deficient cells over MMR-proficient cells. However, observing selective cellular inhibition required micromolar concentrations of these first-generation compounds. Additionally, complexes studied that contained lipophilic ligands to enhance cellular uptake showed a loss of selective cellular toxicity (20, 21). Second-generation complexes containing an N^O coordination and lower overall charge yielded compounds that are selectively cytotoxic toward MMR-deficient cells at nanomolar concentrations. Currently, our leading rhodium metalloinsertor complex, [Rh(chrysi)(phen)(PPO]Cl_2 [Rh-PPO, where phen = 1,10-phenanthroline and PPO = 2-(pyridine-2-yl)propan-2-ol], displays highly potent and selective cytotoxicity toward the MMR-deficient human colorectal cancer cell (CRC) line HCT116O

Significance

This study describes our first evaluation in mice of the rhodium complex Rh-PPO, which selectively targets DNA base-pair mismatches and shows cytotoxicity within mismatch repair-deficient cancer cells. Rh-PPO displays notable in vivo anticancer activity and increases mouse survival when administered intraperitoneally. This work marks the development of a promising metal chemotherapeutic and a new strategy for mismatch-repair-deficient cancers.

Author contributions: S.D.T., T.W.S., J.W., and J.K.B. designed research; S.D.T. and T.W.S. performed research; S.D.T., T.W.S., and J.W. analyzed data; and S.D.T. and J.K.B. wrote the paper.

Reviewers: J.L.S., The University of Texas at Austin; and B.M.Z., Hunter College.

The authors declare no competing interest.

[1]To whom correspondence may be addressed. Email: jkbarton@caltech.edu.

This article contains supporting information online at https://www.pnas.org/lookup/suppl/doi:10.1073/pnas.2006569117/-/DCSupplemental.

First published July 13, 2020.

compared to HCT116N cells, the matched MMR-proficient cell line (22).

Furthermore, a study assessing the cytotoxicity of Rh-PPO in 27 CRC cell lines spanning the four subtypes of CRC, as well as both MMR-deficient and MMR-proficient phenotypes, provided additional support to the hypothesis that the targets of Rh-PPO are DNA base-pair mismatches (23, 24). Rh-PPO was found to be on average five times more potent than the Food and Drug Administration (FDA)–approved chemotherapeutic cisplatin with mean IC_{50} values (50% inhibitory concentration) of 2.9 μM and 13.2 μM, respectively, across CRC cell lines. Specifically, for HCT116O MMR-deficient cells, Rh-PPO displays a half-maximal inhibitory concentration (IC_{50}) of 250 nM compared to 27.5 μM for oxaliplatin, the comparator used in this study. (Scheme 1 shows structures from both generations of metalloinsertors along with oxaliplatin.)

Given the demonstrated significant and selective toxicity toward MMR-deficient cells, and the high cellular potency observed with Rh-PPO, we have continued to explore the potential application of this rhodium metalloinsertor as a targeted chemotherapeutic. Here, we report in vivo pharmacokinetic and efficacy studies evaluating Rh-PPO in an HCT116 xenograft model. The results presented demonstrate that Rh-PPO displays significant anticancer effects and potency in vivo, highlighting the therapeutic potential of this class of metal complexes targeted to bind DNA mismatches.

Results

Evaluation of the Maximum Tolerated Dose for Metalloinsertor Rh-PPO. In order to determine the in vivo anticancer effects of Rh-PPO, the maximum tolerated dose (MTD) of Rh-PPO was assessed in NOD-*scid* IL2Rgamma^{null} (NSG) mice. Mice were treated intraperitoneally (i.p.) with Rh-PPO at 1, 2, 5, and 15 mg drug per kg mouse body weight for up to 10 consecutive days and observed for adverse clinical side effects. During this experiment, the highest dose evaluated, 15 mg·kg^{-1}·d^{-1} (mpk), was found to be lethal within minutes of administration. Mice in the saline group maintained their activity throughout the 10-d study. Mice receiving Rh-PPO at 2 mpk and 5 mpk began displaying notable symptoms of distress and inactivity, such as becoming lethargic, scruffy, and hunched, starting on day 4 and day 2 of the study, respectively; these mice had to be killed before the 10-d study ended. Conversely, mice receiving Rh-PPO at 1 mpk displayed only mild symptoms of distress, including becoming slightly hunched after 6 d of consecutive treatment. Throughout the MTD study, mice in all treatment groups lost body weight in a dose-dependent manner. The MTD for Rh-PPO was determined to be 1 mpk (1.34 μmol/kg); the mice in this dosing group displayed minimal symptoms of distress or inactivity and survived until the end of the study (10 consecutive days of treatment). Given the results of the MTD study, we chose the Rh-PPO dose of 1 mpk given three to four times per week to conduct the subsequent in vivo trial. Rh-PPO is compared to oxaliplatin at 7.5 mpk given twice per week, which is a treatment that has been shown to have notable anticancer effects in HCT116 xenograft tumors (25).

Impact of Rh-PPO on In Vivo Tumor Growth Rate. Two distinct i.p. efficacy experiments with HCT116 xenograft tumors were performed. As outlined in Fig. 1, mice in efficacy experiments 1 and 2 received i.p. doses of metalloinsertor treatments with or without additional saline hydration to assist with drug tolerability, respectively. First, mice were inoculated with HCT116 human colorectal carcinoma cells. Once tumors were palpable at ~100 mm^3 in volume, mice were randomly assigned to each treatment group and drug administration commenced. Mice in efficacy experiments 1 and 2 received the following treatment doses i.p.: Rh-PPO at 0.5 mpk and 1 mpk, oxaliplatin at 7.5 mpk, and vehicle (0.9% NaCl). The doses were administered based on the schedule outlined in Fig. 1. In efficacy experiment 1 mice, subcutaneous (s.c.) administration of 2 mL saline was initiated on the off-treatment days to mitigate the weight loss observed in the first several days of treatment.

As can be seen in Fig. 2, treatment with Rh-PPO yielded a decrease in tumor size. In the groups treated with Rh-PPO in efficacy experiment 1, we observed a significant decrease in tumor growth rate compared to the vehicle control group. By day 21 of the study, the Rh-PPO treatment groups exhibited a 25 ± 2.7% reduction in tumor volume relative to the vehicle treatment group (Fig. 2*A*). This statistically significant reduction in tumor growth rate occurred after mice received four doses of Rh-PPO. Similar decreases in tumor growth were observed in both Rh-PPO treatment groups. Notably, this decrease in tumor volume compared to the control group was sustained for the duration of the study. By the conclusion of the study on day 28, the Rh-PPO– and oxaliplatin-treated groups had statistically similar tumor volumes with oxaliplatin being administered at a 7.5-fold higher dose than Rh-PPO.

Additionally, in the efficacy experiment 2 study, where tumors from each treatment group were all excised on day 28, significant reduction in the final tumor weights was observed (Fig. 2*B*). Specifically, the average tumor weight of the Rh-PPO treatment groups was 24 ± 9.7% lower than the vehicle group and ANOVA analyses of the final tumor weights showed the reduction was statistically significant ($P = 0.03$); this decrease in tumor weight was on par with the reduction observed in oxaliplatin-treated animals. Importantly, neither treatment schedule resulted in significant mouse weight loss (more than 15% of original body weight lost) in the Rh-PPO treatment groups, as shown in Fig. 2*C*, which indicates the metalloinsertor was minimally toxic over the duration of treatment (26).

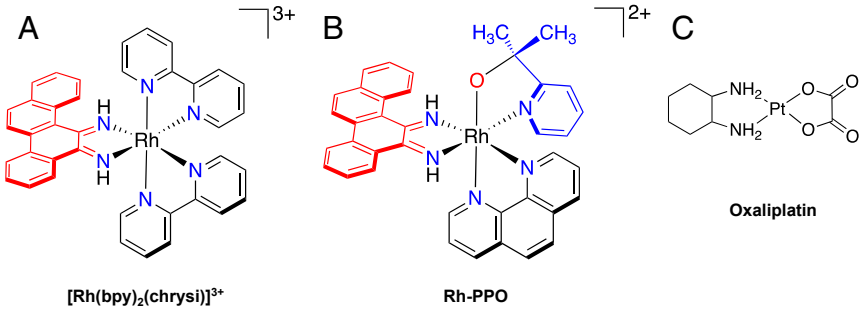

Scheme 1. Chemical structures of compounds used in this study. Chemical structure of (*A*) $[Rh(bpy)_2(chrysi)]^{3+}$, a first-generation metalloinsertor, (*B*) $[Rh(chrysi)(phen)(PPO)]^{2+}$ (Rh-PPO), a second-generation metalloinsertor, and (*C*) oxaliplatin, a widely used FDA-approved chemotherapeutic. The inserting chrysi ligand is shown in red and the axial PPO ligand is displayed in blue.

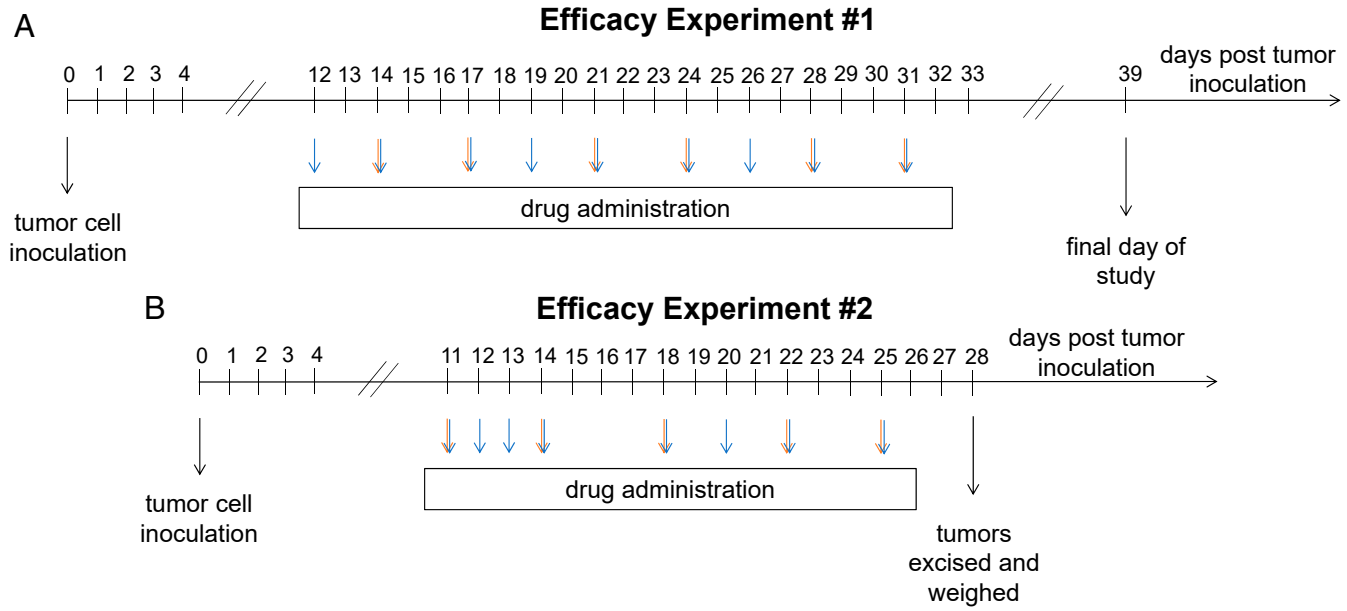

Fig. 1. Drug treatment schedules for Rh-PPO in vivo efficacy experiments with i.p. drug administration. (*A*) Efficacy experiment 1 treatment schedule for the in vivo study monitoring tumor volume and survival rate over time of mice treated i.p. Mice in all treatment groups received 2 mL bolus, s.c., hydrating doses of saline on days 18, 20, 25, 27, and 32. (*B*) Efficacy experiment 2 treatment schedule for the in vivo study assessing final tumor weight of mice receiving i.p. drug treatment. Blue arrow indicates when mice in the saline and Rh-PPO at 0.5 mpk and 1 mpk treatment groups were administered drug doses. Orange/blue double arrows denote when mice in the saline, oxaliplatin at 7.5 mpk, and Rh-PPO at 0.5 mpk and 1 mpk treatment groups were administered drug doses.

Rh-PPO Treatment Influence on Survival Rate of Mice Bearing HCT116 Xenograft Tumors. In order to investigate further the in vivo anticancer efficacy and tolerability of Rh-PPO, we analyzed the survival rates and classified the reason for death of mice in efficacy experiment 1 (Fig. 3). As described above, efficacy experiment 2 instead focused on a tumor weight analysis. Each efficacy experiment 1 treatment group began with 10 to 13 NSG mice bearing HCT116 xenograft tumors. Over the course of the 39-d study, their level of activity and overall health status were monitored. Based on these data, a Kaplan–Meier survival curve (Fig. 3*A*) was constructed for each treatment group from the study (vehicle with 0.9% NaCl, Rh-PPO at 0.5 mpk and 1 mpk, and oxaliplatin at 7.5 mpk). Note the difference in doses for Rh-PPO versus oxaliplatin based on their distinct tolerability and potency.

Mice receiving the Rh-PPO treatment displayed an increase in life span (ILS) of 12% relative to the vehicle control groups (Fig. 3*A*). Additionally, mice in the control group began dying 7 d before those in the Rh-PPO group, with three mice in the vehicle group found dead on day 13 after tumor inoculation, as shown in Fig. 3*A*. Furthermore, classification of the cause of death revealed that 45.5% of saline mouse deaths resulted from mice either being found dead in their cages or killed due to poor health and inactivity (Fig. 3*B*). Conversely, 90% of mice in both Rh-PPO treatment groups died due to their tumors reaching the maximum allowable size (15 mm in diameter). Note that mice in the vehicle group found dead in their cage are assumed to have succumbed to the physical stress of their HCT116 xenograft tumors, while mice in the Rh-PPO and oxaliplatin groups found dead are assumed to have perished due to the combined physical stress of their HCT116 xenograft tumors and the drug treatment. Also, mice killed due to poor health displayed signs of distress, such as having scruffy fur or being hunched for multiple consecutive days before they were killed.

Importantly, the FDA-approved chemotherapeutic oxaliplatin displayed the same ILS of 12% as Rh-PPO but was associated with more toxicity; 45.5% and 18.2% of oxaliplatin mouse deaths resulted from mice being found dead in their cages and mice being killed due to poor health and inactivity, respectively. It should be noted that the death classification analysis was conducted based on mice from efficacy experiment 1 only. Overall, these findings show that Rh-PPO prolongs the survival of mice bearing HCT116 xenograft tumors to a similar extent as oxaliplatin, while also being better tolerated than the platinum complex at their respective MTDs.

Pharmacokinetic Profile of Rh-PPO. Mice from efficacy experiment 1 were further examined to assess the pharmacokinetic profile of Rh-PPO in NSG mice. Fig. 4 summarizes the plasma concentration of the metalloinsertor drug over time during this in vivo analysis. This experiment reveals that the average plasma concentration and bioavailability of Rh-PPO is very similar for both doses tested, which may explain the comparable antitumor effects observed at 0.5 and 1 mpk Rh-PPO. The variation in compound detected at the first time point could indicate the need to take earlier time points in future studies or potentially reflects the variability in clearance rates or drug administration of the different animals evaluated. As shown in the graph, the peak plasma concentration was reached within 30 min of dosing and Rh-PPO was eliminated quickly with elimination half-lives ($t_{1/2}$) of 1.79 h and 1.11 h for the Rh-PPO 1 mpk and Rh-PPO 0.5 mpk dosing groups, respectively. For comparison, the half-life of oxaliplatin is 14.1 min (27). A maximum plasma concentration (C_{max}) of 650 nM for the Rh-PPO 1 mpk cohort was observed, which indicates the exposure level of Rh-PPO in vivo for this dose is ~2.5-fold greater than the in vitro cell IC_{50} value of 250 nM for HCT116 cells (23). Additionally, the area under the curve ($AUC_{0–8\ h}$) value was calculated based on the plasma concentration curve as summarized in Table 1. Importantly, Rh-PPO concentration was determined by liquid chromatography–tandem mass spectrometry (LC-MS/MS); therefore, the measured drug levels represent detection of the intact Rh-PPO complex.

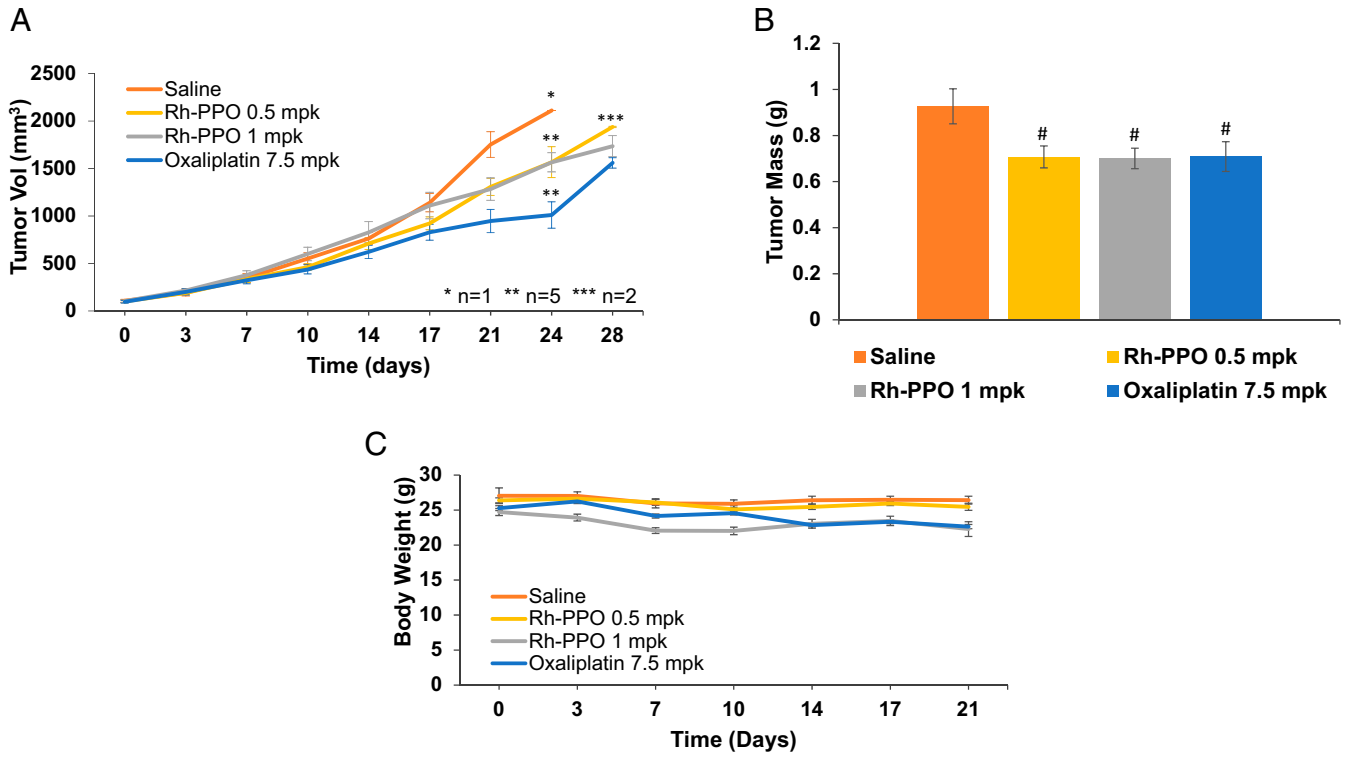

Fig. 2. Rh-PPO tolerability and impact on in vivo tumor growth rate. (*A*) Average tumor volumes of efficacy experiment 1 mice receiving i.p. doses throughout the dosing period. Number of mice: $*n = 1$, $**n = 5$, $***n = 2$. (*B*) Average final tumor weights for efficacy experiment 2 mice. Tumors were excised after 18 d of treatment with 8 to 10 tumors collected and analyzed per treatment group. Statistically significant difference between treatment groups and saline control was found based on ANOVA analysis; $^{\#}P < 0.05$ ($^{\#}P = 0.03$). (*C*) Efficacy experiment 1 average mouse body weights over time after treatment commenced ($n = 8$ to 11 mice). All error bars represent SEM.

At the conclusion of each efficacy study, the tumors along with various organs were collected and analyzed for rhodium and platinum content (Fig. 5) using inductively coupled plasma MS (ICP-MS). This high-sensitivity technique allows for the detection of low concentrations of metal-based drugs (less than 1 ng/mL) and background levels of rhodium and platinum can be detected in the saline treatment group (28). Importantly, the tumor and organ samples underwent distinct nitric acid digestion protocols (see Experimental Section), and therefore metal content in the tumors and organs cannot be directly compared. Nonetheless, the results collected from ICP-MS studies indicate that a significant amount of both drugs, Rh-PPO and oxaliplatin, became distributed to various organs as opposed to being directed selectively to the site of the tumors. Notably, when comparing the tumor-to-normal-tissue ratio for both drugs, a higher proportion of platinum was localized to tumors in the oxaliplatin-treated mice. Additionally, dose-dependent accumulation of rhodium was detected in the analyzed i.p. treated

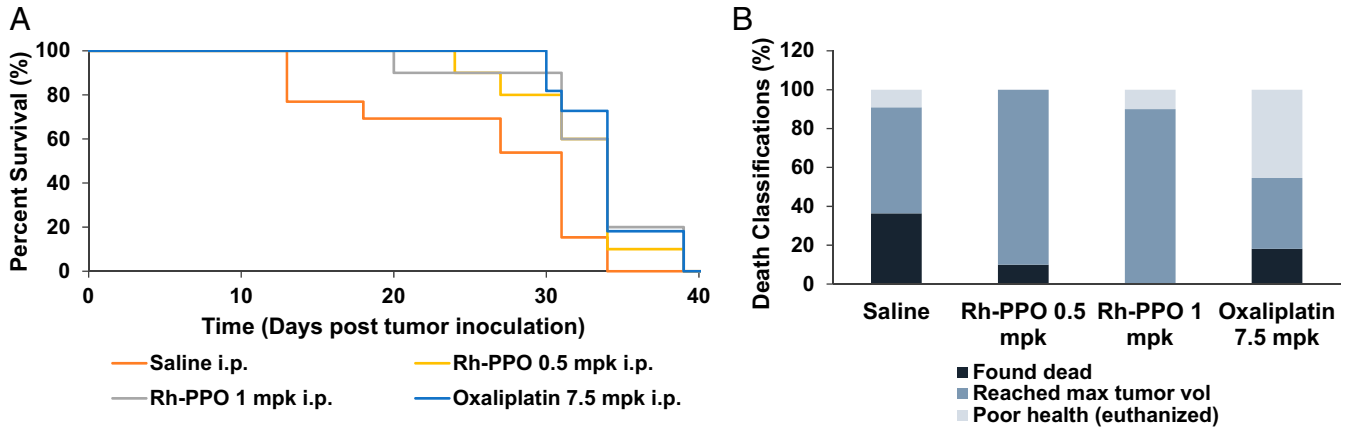

Fig. 3. Rh-PPO treatment increases mouse survival rate. (*A*) Kaplan–Meier survival curve for efficacy experiment 1 mice. Mice were considered dead if found dead in their cage, mouse health warranted killing, or tumor diameter surpassed 15 mm. (*B*) Classification of reason for mouse deaths. Black indicates mice were found dead. Blue-gray represents mice that were killed due to their tumor reaching the maximum allowable size (15 mm in diameter). Light gray denotes mice had to be killed due to poor health. Bar graph displays percentage of mice that died for each outlined reason.

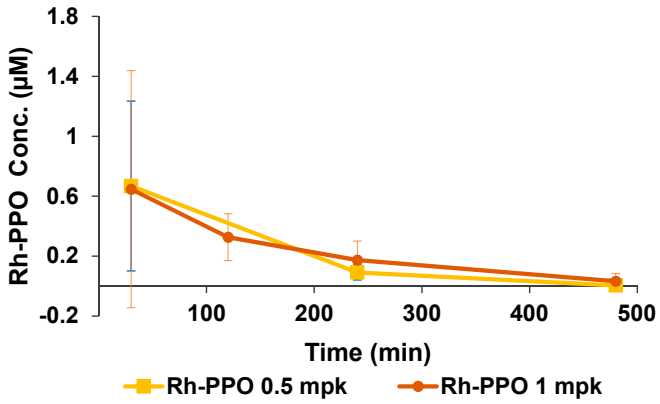

Fig. 4. Pharmacokinetic profile of Rh-PPO after i.p. drug administration. Concentration of Rh-PPO in mouse plasma of efficacy experiment 1 animals ($n = 2$ or 3) dosed i.p. with Rh-PPO at 0.5 mpk and 1 mpk. Amount of intact Rh-PPO detected in mouse plasma was analyzed via LC-MS/MS at various time points up to 4 h after a single, i.p. bolus dose was administered.

tumors. It should be noted that for the i.p. efficacy studies ninefold less rhodium was present in Rh-PPO tumors compared to platinum levels in oxaliplatin-treated mice, despite similar anticancer effects being observed for the two drugs; this result reflects the higher potency of the rhodium complex. Furthermore, the tissue analysis of oxaliplatin-treated animals showed platinum was distributed evenly (within the SE) for all organs analyzed.

Additionally, Rh content (Fig. 5*B*) and histological analyses of the tissues collected showed normal organ morphology in Rh-PPO–treated mice with accumulation of rhodium most significantly in the liver (1 ng [Rh]/mg tissue = 9.7×10^{-9} mol [Rh]/kg tissue). This tissue analysis gives insight into the potential mechanisms of Rh-PPO clearance and currently suggests that Rh-PPO is most readily cleared through the liver and the incorporation of saline hydrating doses likely decreased the overall rhodium concentration in the kidneys. Overall, these findings support our analysis that Rh-PPO was sufficiently tolerated throughout the study and displays an expected pharmacokinetic profile (29). However, increased efficacy will require more selective delivery of Rh-PPO to the tumor versus healthy organs.

Impact of Intratumoral Rh-PPO Treatment on In Vivo Tumor Growth. In addition to the two efficacy studies detailed above, in which Rh-PPO was administered i.p., we also explored the antitumor effects observed with Rh-PPO intratumoral treatment. The intratumoral efficacy experiment gave insight into the antiproliferative potential of Rh-PPO if the complex is specifically targeted to the site of the tumor. As shown in Fig. 6, intratumoral doses of Rh-PPO at 1 mpk displayed a 40% reduction in tumor volume, as well as 49% lower average tumor weights ($P = 0.002$), compared to the saline control after only 7 d of treatment (0.142 mg Rh-PPO total administered). These results indicate that reductions to tumor growth can be doubled in one-third the time frame when the treatment is administered directly to the tumor compared to i.p. injections. Additionally, this increased level of anticancer activity was strongly correlated with enhanced levels of rhodium in tumors detected by ICP-MS; specifically, tumors from intratumorally treated mice had 50-fold higher rhodium concentrations at the tumor site compared to the i.p. treatment groups (*SI Appendix*, Fig. S2). It should be noted that intratumoral doses were only given for 7 d because this administration route resulted in significant systemic toxicity, including mouse inactivity and notable weight loss.

Discussion

Platinum complexes have been extensively studied and utilized as chemotherapeutics (30), where these compounds aim to target DNA within rapidly dividing malignant cells. However, these complexes are associated with adverse effects and patients frequently develop resistance to these treatments (8–10). As a result, we have focused on the development of targeted chemotherapeutics for DNA with improved selectivity for cancerous cells, specifically for MMR-deficient cancers, which have underdeveloped treatment options currently.

We have designed and characterized rhodium metalloinsertors which bind specifically to DNA mismatches and as a result induce selective toxicity within MMR-deficient cancer cell lines (16, 22, 23, 31–33). In addition, various ruthenium complexes have been designed and synthesized as chemotherapeutics, although with different biological targets (21, 34–36). The high potency and demonstrated biological selectivity of Rh-PPO for DNA mismatches and MMR-deficient cells distinguish it from most other metal chemotherapeutics.

Given the cell-selective cytotoxicity and potency of the Rh-PPO metalloinsertor, the in vivo anticancer activity of the complex was evaluated in NSG mice with human colorectal carcinoma HCT116 xenograft tumors. Initial experiments that showcased the high aqueous solubility of the complex and stability of Rh-PPO in rat plasma and rat liver microsomes for up to 4 h supported the transition toward preclinical studies with Rh-PPO. Our first mouse experiments aimed to explore the administration route (oral, intravenous [i.v.], s.c., i.p., etc.) best suited for achieving tolerable, systemic chemotherapeutic effects with the metalloinsertor complex. These studies showed Rh-PPO effectively had zero oral bioavailability and i.v. administration of the metalloinsertor at 20 mpk was not well tolerated; therefore, alternative administration routes and drug concentrations were explored. The MTD study described in this work revealed that bolus, i.p. injections of Rh-PPO at 1 mpk are tolerated over a 10-d period with minor indications of systemic toxicity. Additionally, initial pharmacokinetic studies using continuous s.c. infusions (*SI Appendix*, Fig. S1) suggested that supplemental injections of saline promoted the clearance of Rh-PPO and increased overall tolerability of the drug; therefore, supplemental saline hydration was incorporated into the in vivo study design, as described in Fig. 1. With the MTD and dose administration conditions for Rh-PPO determined, we continued with the preclinical evaluation of this metalloinsertor compound as a targeted chemotherapeutic.

The present study evaluates the in vivo tolerability, cytotoxic tumor effects, and pharmacokinetic properties of the metalloinsertor Rh-PPO. Analysis of tumor growth in the two i.p., efficacy experiments demonstrates statistically significant differences in tumor volume and final tumor mass between the i.p. vehicle and Rh-PPO treatment groups. Specifically, an ANOVA test of the final tumor weights obtained from efficacy experiment 2 mice reveal a decrease in average tumor weights of $24 \pm 9.7\%$ for both Rh-PPO treatment groups ($P = 0.03$), which is comparable to the decrease in HCT116 tumor weight observed in mice treated with oxaliplatin. Importantly, while platinum complexes are generally less effective in MMR-deficient cells, our in vivo experiments with Rh-PPO were conducted alongside

Table 1. Pharmacokinetic parameters of Rh-PPO after i.p. drug administration

Pharmacokinetic parameter	Rh-PPO 0.5 mpk	Rh-PPO 1 mpk
C_{max}, μM	0.45	0.65
$t_{1/2}$, h	1.11	1.79
$AUC_{0–8\ h}$, μM × h	1.31	1.52

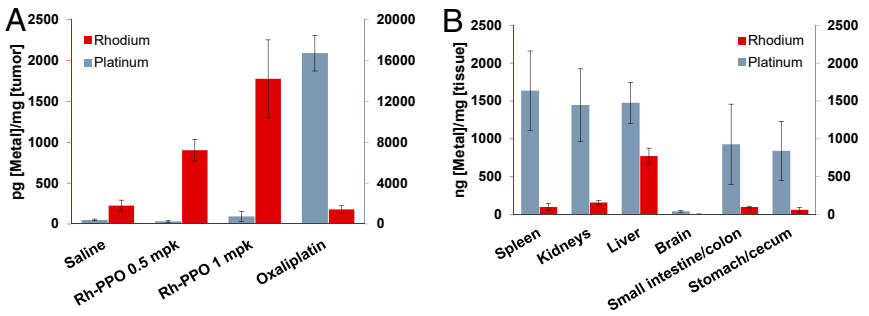

Fig. 5. Accumulation of Rh and Pt in tissues after i.p. drug treatment. (*A*) Rhodium and platinum uptake in HCT116 xenograft tumors of efficacy experiment 2 mice. Rhodium and platinum accumulation in tumors was determined using ICP-MS analysis of tumors digested in nitric acid and normalized to initial tumor weight. The rhodium and platinum concentrations detected in tumors from each treatment group (n = 9 or 10) were averaged. (*B*) Rhodium and platinum uptake in various tissues collected from efficacy experiment 1 mice. Rhodium accumulation was determined using ICP-MS analysis of digested tissue samples collected from mice treated with Rh-PPO at 1 mpk. Platinum accumulation was determined using ICP-MS analysis of digested tissue samples collected from mice treated with oxaliplatin at 7.5 mpk. Metal concentrations were normalized to initial tissue weight. The metal concentrations detected in organs from each treatment group were averaged (n = 2 to 4). Error shown as the SEM.

oxaliplatin because previous studies have demonstrated this compound has antiproliferative effects in HCT116 xenograft tumors and colon cancer cells generally (25).

Reduction in tumor growth from Rh-PPO administration was also evident based on the tumor volume analysis conducted in efficacy experiment 1, which clearly showed a decrease in tumor growth rate starting on day 21 of the study. In particular, Rh-PPO–treated tumors were 25 ± 2.7% smaller than the control group mean tumor volume. Additionally, analysis of the survival rates in the first efficacy experiment showed a 12% ILS for metalloinsertor-treated animals compared to the vehicle-treated group. Furthermore, Rh-PPO was found to be less systemically toxic than oxaliplatin, as 10% and 45% of Rh-PPO– (1 mpk) and oxaliplatin-treated animals had to be killed due to poor health and inactivity, respectively. Moreover, Rh-PPO was shown to be significantly more potent than oxaliplatin in vivo, as ninefold lower metal concentrations were necessary, as shown by ICP-MS analysis of tumors, to cause similar anticancer effects with the two drugs (Fig. 5*A*). Additionally, we assessed the tumor growth effects when Rh-PPO was administered through intratumoral injection and found greater than 40% reductions in tumor volume and weight after only 7 d of treatment. The intratumoral route of administration was also found to be unacceptably toxic, most likely due to rapid increases in systemic Rh-PPO concentrations similar to those achieved with i.v. dosing. Importantly, this experiment clearly indicates that when more complex becomes specifically localized to the tumor site in vivo significantly greater anticancer effects are observed.

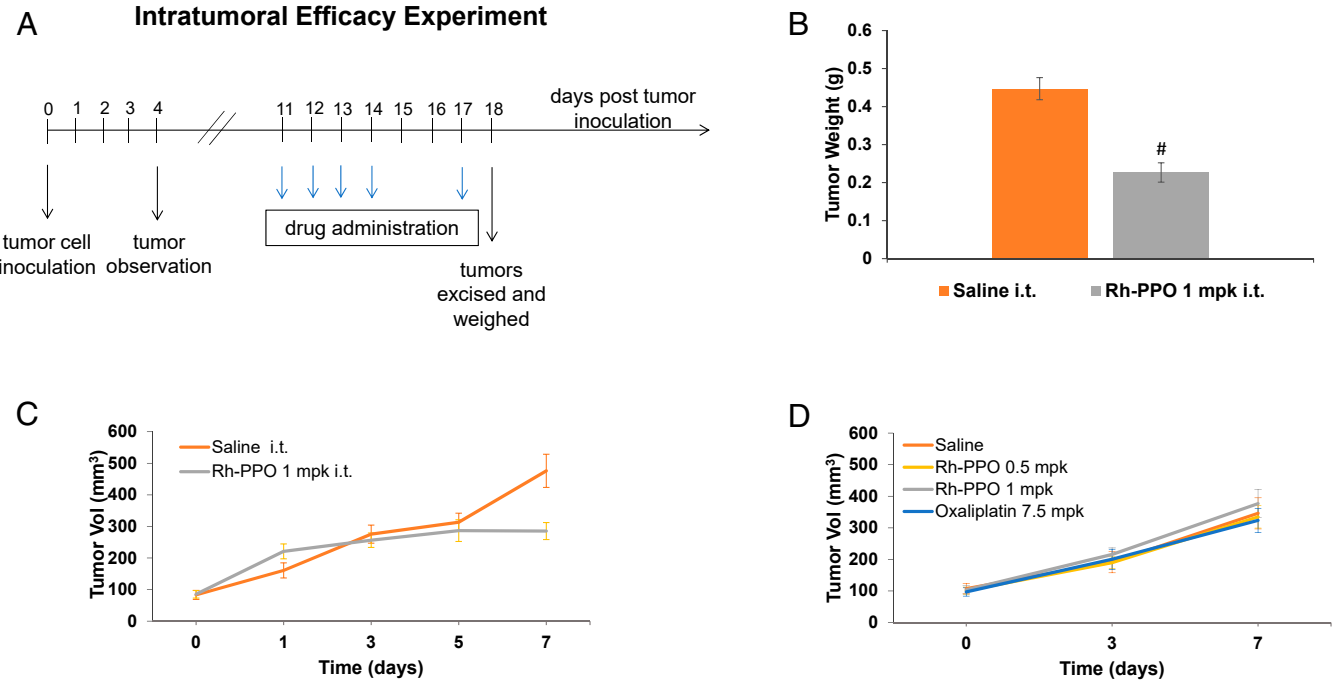

Fig. 6. Intratumoral Rh-PPO treatment causes in vivo tumor growth rate to decrease rapidly. (*A*) Intratumoral efficacy experiment treatment schedule for study monitoring tumor volume and final tumor weight in mice treated intratumorally. Blue arrow indicates mice received intratumoral drug doses of saline and Rh-PPO at 1 mpk. (*B*) Average final tumor weights for intratumoral-treated mice. Tumors were collected after 7 d of treatment. (*C*) Evaluation of the average tumor volume over the first 7 d of treatment in cohorts receiving intratumoral and (*D*) i.p. drug doses. Error bars represent SEM. Statistically significant difference between the final tumor weights of Rh-PPO and saline treatment groups was found using ANOVA test; $^{\#}P < 0.005$ ($P = 0.002$).

In order to assess further the preclinical potential of Rh-PPO, pharmacokinetic analyses of plasma samples collected from mice receiving i.p. doses of Rh-PPO were conducted. These experiments revealed that the half-life of the compound is in the range expected for a chemotherapeutic (1.11 h to 1.79 h depending on the dose). Additionally, the pharmacokinetic curve obtained demonstrates a C_{max} that is above the IC_{50} of Rh-PPO (250 nM in HCT116 cells) for both doses assessed, consistent with the antitumor efficacy observed in vivo (23). Tumor and tissue analyses revealed a dose-dependent accumulation of rhodium within the tumors of Rh-PPO–treated mice; however, a higher distribution of rhodium to the liver compared to the tumor and other organs was observed. The rhodium liver accumulation detected could be indicative of Rh-PPO undergoing hepatic drug clearance. This differs greatly from oxaliplatin, which showcased equal distribution of platinum in the different organs analyzed, with the exception of the brain, which is consistent with reports of oxaliplatin's being cleared by a combination of tissue binding and renal clearance (37, 38). Comparing the concentrations of rhodium/platinum measured within tumors and tissues revealed significant amounts of drug are becoming absorbed within healthy tissues, which underscores the need for Rh-PPO to be further targeted to the site of tumors for its full chemotherapeutic potential to be achieved.

In summary, we report that significant antiproliferative effects in colorectal carcinoma HCT116 xenograft tumors are observed when Rh-PPO is administered via i.p. injection, and these antitumor effects are on par with oxaliplatin treatment. Tumor growth in Rh-PPO–treated mice is notably slowed in the described efficacy experiments. However, tumor cell proliferation is ultimately not eliminated. Furthermore, while the i.p. administration route did not result in detrimental systemic toxicity during the outlined treatment period, accumulation of rhodium in organs is likely to cause long-term, toxic side effects. Results from the intratumoral Rh-PPO study indicate that higher localization of compound to the site of the tumor should result in even greater anticancer effects. In order to mitigate the systemic toxicity of Rh-PPO observed at higher concentrations and increase cytotoxic effects at the tumor site, it will be important to explore different approaches to drug delivery that may further target metalloinsertor complexes to tumors more efficiently. This study reports an in vivo analysis of DNA mismatch-targeted rhodium metalloinsertors, and the anticancer effects observed validate these compounds as potential chemotherapeutic agents that warrant further investigation.

Materials and Methods

General Procedures. All chemicals, reagents, and solvents used for synthesis were commercially available, unless otherwise noted, and used as received. Organic solvents were purchased from Sigma-Aldrich unless otherwise noted. Water was purified using the Millipore Milli-Q system. [Rh(chrysi)(phen)(2-(pyridine-2-yl)propan-2-ol]Cl_2 (Rh-PPO) and [Rh(chrysi)(phen)(1-Phenyl-1-(pyridine-2-yl)ethan-1-ol.]Cl_2 (Rh-PPE) were synthesized following published methodology (22). Oxaliplatin was purchased from Alfa Aesar. High-performance LC (HPLC)–grade acetonitrile and methanol were purchased from Fisher Scientific. Formic acid (99% pure) was purchased from Acros Organic. Sep-Pak C18 solid-phase extraction cartridges were acquired from Waters Chemical Co. All HPLC metal complex purifications were carried out on a Hewlett-Packard 1100 HPLC. All ultraviolet-visible (UV-Vis) spectroscopic experiments were performed on a Cary 100 spectrometer. Cell culture media and supplements were purchased from Life Technologies. Cell lines used in the experiment were purchased from ATCC. Tissue culture flasks and plates were obtained from Corning.

Cell Culture. HCT116 cells were grown and maintained using McCoy's 5A (modified) media supplemented with 10% fetal bovine serum (FBS) and 100 units/mL penicillin and streptomycin. The cells were incubated in tissue culture flasks at 37 °C in a 5% CO_2 atmosphere. Standard procedures for entering and exiting cryostorage were followed, as well as methods for subculturing HCT116 cells. Cell solutions of 2.5×10^6 cells per 100 μL media were made for tumor inoculation using only McCoy's 5A (modified) media supplemented with 10% FBS.

Mice Preclinical Assessment Studies. All animal experiments were done in accordance with protocols approved by the Institutional Animal Care and Use Committees at City of Hope. All experiments were performed in accordance with the City of Hope policies on the care, welfare, and treatment of laboratory animals. For all experiments, NSG mice from City of Hope Animal Resources Center were used. Each cage contained up to four mice and animals were offered standard diet and water. All animal studies were performed with the chloride salt of the metalloinsertor. Rh-PPO and Rh-PPE concentrations were determined by UV-Vis using the extinction coefficients of the complex (*SI Appendix*) (22).

MTD Studies. NSG mice were weighed then received i.p. injections of Rh-PPO dissolved in saline at concentrations of 1, 2, 5, or 15 mpk; i.p. injections were administered once daily for 10 consecutive days. Clinical observations were made daily and mouse body weights were recorded. At the end of the study, surviving animals were killed using carbon dioxide.

In Vivo Tumor Growth Inhibition and Survival Rate. NSG mice, weighing 23 to 34 g, were injected s.c. in the right flank with 100 μL HCT116 cells (2.5×10^6 cells) suspended in McCoy's media. Tumors were allowed to grow until they reached ~100 mm^3, 11 to 12 d after tumor inoculation. Tumor volumes (TV) were estimated by measuring the width (W) and length (L) of the tumor using a digital caliper and calculated based on the following formula: $TV = W^2L/2$ (39).

In Vivo Efficacy Experiments. Mice were randomly assigned to each treatment group, such that each group had 10 to 13 mice and an average tumor volume of ~100 mm^3. Mice were allocated to the following treatment groups: vehicle (0.9% NaCl), Rh-PPO at 0.5 mpk, Rh-PPO at 1 mpk, and oxaliplatin at 7.5 mpk. Rh-PPO was dissolved in saline at the MTD (1 mpk) and MTD/2 (0.5 mpk) and administered intraperitoneally three or four times per week. Saline was administered intraperitoneally to the control group three or four times per week. Clinical-grade oxaliplatin (Alfa Aesar) was dissolved in 5% dextrose using sonication and administered i.p. two times per week, as reported in previous studies (25). Two in vivo, i.p. efficacy experiments were conducted, and the specific dosing schedules for each study and treatment group are outlined in Fig. 1. Mouse body weights and tumor volumes were measured twice per week over the course of each study.

Efficacy Experiment 1. This study contained the following number of mice per dosing group: saline ($n = 13$), Rh-PPO at 0.5 mpk ($n = 10$), Rh-PPO at 1 mpk ($n = 10$), and oxaliplatin at 7.5 mpk ($n = 11$). As described in Fig. 1, mice in all treatment groups in efficacy experiment 1 received 2 mL bolus, s.c. injections of saline twice per week in order to increase drug tolerability (days 18, 20, 25, 27, and 32). The specific dosing schedule for each treatment group in efficacy experiment 1 is outlined in Fig. 1*A*.

Efficacy Experiment 2. This study contained 10 mice in each treatment group. The specific dosing schedule for each treatment group in efficacy experiment 2 is outlined in Fig. 1*B*. Note that the drug dosing schedule was altered after day 14 to increase tolerability of Rh-PPO.

Survival Rate Studies. Survival rate was determined by comparing the number of animals alive at different time points during the study to the total number of animals at the start of the study. Mice were removed from the study if they were found dead in their cage, declining health necessitated killing, or tumor diameter exceeded 15 mm. These parameters were used to construct a Kaplan–Meier survival curve. ILS was calculated based on the following equation: $ILS = (Days_T - Days_C)/Days_C$, where $Days_C$ = days survived by control group mice and $Days_T$ = days survived by treatment group mice. ILS was determined to compare the survival rates of the different treatment groups. Each treatment group started with 10 to 13 mice. After treatment completion, mice were killed using carbon dioxide, and tumors were dissected and weighed. In three mice per treatment group in efficacy experiment 1, major organs (spleen, kidneys, liver, heart, skeletal muscle, lungs, small intestine, colon, stomach, cecum, testes, epididymis, tumor, tibia/femur, and brain) were harvested and cut in half; one half was fixed in 10% formalin and the other half frozen on dry ice for further analysis.

Tumor Weight Analysis. In efficacy experiment 2, 18 d after starting treatment all mice were killed using carbon dioxide and HCT116 xenograft tumors were dissected, weighed, and frozen on dry ice. Tumor weights were analyzed using the ANOVA test to determine the significance of the results. In three

mice per treatment group in efficacy experiment 2, major organs (spleen, kidneys, liver, heart, skeletal muscle, lungs, small intestine, colon, stomach, cecum, testes, epididymis, tumor, tibia/femur, and brain) were harvested and cut in half; one half was fixed in 10% formalin and the other half frozen on dry ice for further analysis.

Pharmacokinetic Studies.

Determination of Rh-PPO in vivo biodistribution. In efficacy experiment 1, after the final Rh-PPO drug dose was administered, blood was collected via cardiac puncture using a syringe and immediately transferred to heparinized blood collection vials on ice at time intervals of 0.5, 1, 2, 4, and 8 h post-administration (three mice per Rh-PPO treatment group per time point). The blood samples were centrifuged at 15,000 × *g* at room temperature for 5 min, and the supernatant plasma was transferred to 1.5-mL micro-centrifuge tubes and maintained at −80 °C until analysis. Plasma samples were prepared for LC-MS/MS analysis by mixing 20 μL mouse plasma sample with 10 μL 50% acetonitrile in water in a 0.5-mL low-retention micro-centrifuge tube. Then, 100 μL of 500ng/mL Rh-PPE internal standard in acetonitrile was added to the sample tube and the solution was vortexed for 3 min. The sample was then centrifuged at 14,800 × *g* for 5 min at 4 °C and 20 μL of the resulting supernatant was mixed with 180 μL 25% acetonitrile in 10 mM NH_4OAC buffer (pH 3.2). Finally, 2 μL of the resulting sample was analyzed via LC-MS/MS (*SI Appendix*).

Tissue Digestion Analysis. Mice from efficacy experiment 2 bearing HCT116 xenografts that were treated with Rh-PPO and oxaliplatin were used for the following analyses. Prior testing was performed using chicken liver incubated with Rh or Pt standards to assess nitric acid digestion protocol accuracy in detecting rhodium and platinum using ICP-MS.

Tumor digestion analysis. Tumors were collected, weighed, frozen at −80 °C overnight, then dried using the lyophilizer for over 3 d. Lyophilized tumor samples were then immediately manually homogenized using a metal spatula and reweighed. The homogenized tumors were transferred to 50-mL Digitubes and 2 mL of 25% HNO_3 was added to each sample. The sample was then covered with a watch glass and heated to 100 °C on a DigiPREP block digestion system for 24 h. The digested tumor samples were centrifuged for 5 min at 1,000 rpm. Supernatant (200 μL) was transferred to new 15-mL Falcon tubes containing 4.8 mL H_2O. The diluted sample (1% HNO_3) was centrifuged for 5 min at 1,500 rpm and analyzed by ICP-MS for Rh^{103} and Pt^{195}.

Organ digestion analysis. The collected organs were weighed and transferred to 50-mL Digitubes, to which 2 to 5 mL of concentrated HNO_3 (68%) was added. The tubes were then covered with a watch glass and heated to 100°C on a DigiPREP block until the sample was fully digested (2 to 8 h). The digested tissue samples were evaporated using gentle heating at 65 °C until ∼1 mL of sample remained. Then, a 2% HNO_3 (aqueous) solution was added to each sample to reach a final volume of 25 mL. The resulting samples were analyzed by ICP-MS for Rh^{103} and Pt^{195}.

Data Availability. The raw data for the outlined experiments are available in *SI Appendix*.

ACKNOWLEDGMENTS. We are grateful to the NIH for their long-term support of this research (GM33309 to J.K.B.). We thank Dr. Julie Bailis and Dr. Kelsey Boyle for participating in useful discussions that assisted with the design of this study, as well as Dr. Nathan Dalleska from the Environmental Analysis Center at California Institute of Technology for assistance with the ICP-MS analysis. We also thank Yuming Guo for technical assistance. This work was also performed in the City of Hope Analytical Pharmacology Core Facility supported by the National Cancer Institute under Grant P30CA033572.

1. D. B. Zamble, S. J. Lippard, Cisplatin and DNA repair in cancer chemotherapy. *Trends Biochem. Sci.* **20**, 435–439 (1995).
2. P. C. Bruijnincx, P. J. Sadler, New trends for metal complexes with anticancer activity. *Curr. Opin. Chem. Biol.* **12**, 197–206 (2008).
3. N. Muhammad, Z. Guo, Metal-based anticancer chemotherapeutic agents. *Curr. Opin. Chem. Biol.* **19**, 144–153 (2014).
4. A. C. Komor, J. K. Barton, The path for metal complexes to a DNA target. *Chem. Commun. (Camb.)* **49**, 3617–3630 (2013).
5. L. Kelland, The resurgence of platinum-based cancer chemotherapy. *Nat. Rev. Cancer* **7**, 573–584 (2007).
6. K. Cheung-Ong, G. Giaever, C. Nislow, DNA-damaging agents in cancer chemotherapy: Serendipity and chemical biology. *Chem. Biol.* **20**, 648–659 (2013).
7. S. Capra, M. Ferguson, K. Ried, Cancer: Impact of nutrition intervention outcome–nutrition issues for patients. *Nutrition* **17**, 769–772 (2001).
8. S. Dasari, P. B. Tchounwou, Cisplatin in cancer therapy: Molecular mechanisms of action. *Eur. J. Pharmacol.* **740**, 364–378 (2014).
9. E. Martinez-Balibrea *et al*., Tumor-related molecular mechanisms of oxaliplatin resistance. *Mol. Cancer Ther.* **14**, 1767–1776 (2015).
10. D. W. Shen, L. M. Pouliot, M. D. Hall, M. M. Gottesman, Cisplatin resistance: A cellular self-defense mechanism resulting from multiple epigenetic and genetic changes. *Pharmacol. Rev.* **64**, 706–721 (2012).
11. A. G. Weidmann, A. C. Komor, J. K. Barton, Targeted chemotherapy with metal complexes. *Comments Mod. Chem. A Comments Inorg. Chem.* **34**, 114–123 (2014).
12. Z. Li, A. H. Pearlman, P. Hsieh, DNA mismatch repair and the DNA damage response. *DNA Repair (Amst.)* **38**, 94–101 (2016).
13. I. I. Arzimanoglou, F. Gilbert, H. R. Barber, Microsatellite instability in human solid tumors. *Cancer* **82**, 1808–1820 (1998).
14. S. B. Hatch *et al*., Microsatellite instability testing in colorectal carcinoma: Choice of markers affects sensitivity of detection of mismatch repair-deficient tumors. *Clin. Cancer Res.* **11**, 2180–2187 (2005).
15. P. Zhao, L. Li, X. Jiang, Q. Li, Mismatch repair deficiency/microsatellite instability-high as a predictor for anti-PD-1/PD-L1 immunotherapy efficacy. *J. Hematol. Oncol.* **12**, 54 (2019).
16. K. M. Boyle, J. K. Barton, Targeting DNA mismatches with rhodium metalloinsertors. *Inorg. Chim. Acta* **452**, 3–11 (2016).
17. S. K. Fung *et al*., Luminescent platinum(II) complexes with functionalized N-heterocyclic carbene or diphosphine selectively probe mismatched and abasic DNA. *Nat. Commun.* **7**, 10655 (2016).
18. B. M. Zeglis, V. C. Pierre, J. T. Kaiser, J. K. Barton, A bulky rhodium complex bound to an adenosine-adenosine DNA mismatch: General architecture of the metalloinsertion binding mode. *Biochemistry* **48**, 4247–4253 (2009).
19. B. M. Zeglis, V. C. Pierre, J. K. Barton, Metallo-intercalators and metallo-insertors. *Chem. Commun. (Camb.)* **44**, 4565–4579 (2007).
20. R. J. Ernst, A. C. Komor, J. K. Barton, Selective cytotoxicity of rhodium metalloinsertors in mismatch repair-deficient cells. *Biochemistry* **50**, 10919–10928 (2011).
21. A. C. Komor, C. J. Schneider, A. G. Weidmann, J. K. Barton, Cell-selective biological activity of rhodium metalloinsertors correlates with subcellular localization. *J. Am. Chem. Soc.* **134**, 19223–19233 (2012).
22. A. C. Komor, J. K. Barton, An unusual ligand coordination gives rise to a new family of rhodium metalloinsertors with improved selectivity and potency. *J. Am. Chem. Soc.* **136**, 14160–14172 (2014).
23. K. M. Boyle, A. Nano, C. Day, J. K. Barton, Cellular target of a rhodium metalloinsertor is the DNA base pair mismatch. *Chemistry* **25**, 3014–3019 (2019).
24. J. Guinney *et al*., The consensus molecular subtypes of colorectal cancer. *Nat. Med.* **21**, 1350–1356 (2015).
25. L. M. Howells *et al*., Curcumin ameliorates oxaliplatin-induced chemoresistance in HCT116 colorectal cancer cells in vitro and in vivo. *Int. J. Cancer* **129**, 476–486 (2011).
26. W. J. Aston *et al*., A systematic investigation of the maximum tolerated dose of cytotoxic chemotherapy with and without supportive care in mice. *BMC Cancer* **17**, 684 (2017).
27. T. Alcindor, N. Beauger, Oxaliplatin: A review in the era of molecularly targeted therapy. *Curr. Oncol.* **18**, 18–25 (2011).
28. B. J. Perry, R. E. Balazs, ICP-MS method for the determination of platinum in suspensions of cells exposed to cisplatin. *Anal. Proc. Incl. Anal. Commun.* **31**, 269–271 (1994).
29. M. Frik *et al*., In vitro and in vivo evaluation of water-soluble iminophosphorane ruthenium(II) compounds. A potential chemotherapeutic agent for triple negative breast cancer. *J. Med. Chem.* **57**, 9995–10012 (2014).
30. A. Jemal *et al*., Global cancer statistics. *CA Cancer J. Clin.* **61**, 69–90 (2011).
31. K. M. Boyle, J. K. Barton, A family of rhodium complexes with selective toxicity toward mismatch repair-deficient cancers. *J. Am. Chem. Soc.* **140**, 5612–5624 (2018).
32. A. Nano *et al*., Cell-selective cytotoxicity of a fluorescent rhodium metalloinsertor conjugate results from irreversible DNA damage at base pair mismatches. *Biochemistry* **59**, 717–726 (2020).
33. J. M. Bailis, A. G. Weidmann, N. F. Mariano, J. K. Barton, Rhodium metalloinsertor binding generates a lesion with selective cytotoxicity for mismatch repair-deficient cells. *Proc. Natl. Acad. Sci. U.S.A.* **114**, 6948–6953 (2017).
34. J. Coverdale, T. Laroiya-McCarron, I. Romero-Canelón, Designing ruthenium anticancer drugs: What have we learnt from the key drug candidates? *Inorganics (Basel)* **7**, 1–15 (2019).
35. A. Bergamo, A. Masi, P. J. Dyson, G. Sava, Modulation of the metastatic progression of breast cancer with an organometallic ruthenium compound. *Int. J. Oncol.* **33**, 1281–1289 (2008).
36. C. S. Gondi, J. S. Rao, Cathepsin B as a cancer target. *Expert Opin. Ther. Targets* **17**, 281–291 (2013).
37. M. A. Graham *et al*., Clinical pharmacokinetics of oxaliplatin: A critical review. *Clin. Cancer Res.* **6**, 1205–1218 (2000).
38. F. Lévi, G. Metzger, C. Massari, G. Milano, Oxaliplatin: Pharmacokinetics and chronopharmacological aspects. *Clin. Pharmacokinet.* **38**, 1–21 (2000).
39. M. M. Jensen, J. T. Jørgensen, T. Binderup, A. Kjaer, Tumor volume in subcutaneous mouse xenografts measured by microCT is more accurate and reproducible than determined by 18F-FDG-microPET or external caliper. *BMC Med. Imaging* **8**, 16 (2008).